Original Article

MOLECULAR METABOLISM

# Ketogenic diets composed of long-chain and medium-chain fatty acids induce cardiac fibrosis in mice

**Felix Sternberg [1,*], Christina Sternberg [2], Andreas Dunkel [3], Taraneh Beikbaghban [1], András Gregor [4], Aleksander Szarzynski [1], Veronika Somoza [3,5,6], Ingrid Walter [7], Kalina Duszka [4], Barbara Kofler [8], Elena E. Pohl [1,**]**

## ABSTRACT

**Purpose:** Heart diseases are the leading cause of death worldwide. Metabolic interventions via ketogenic diets (KDs) have been used for decades to treat epilepsy, and more recently, also diabetes and obesity, as common comorbidities of heart diseases. However, recent reports linked KDs, based on long-chain triglycerides (LCTs), to cardiac fibrosis and a reduction of heart function in rodents. As intervention using medium-chain triglycerides (MCTs) was recently shown to be beneficial in murine cardiac reperfusion injury, the question arises as to what extent the fatty acid (FA)-composition in a KD alters molecular markers of FA-oxidation (FAO) and modulates cardiac fibrotic outcome.

**Methods:** The effects of LCT-KD as well as an LCT/MCT mix (8:1 ketogenic ratio) on cardiac tissue integrity and the plasma metabolome were assessed in adult male C57/BL6NRJ mice after eight weeks on the respective diet.

**Results:** Both KDs resulted in increased amount of collagen fibers and cardiac tissue was immunologically indistinguishable between groups. MCT supplementation resulted in i) profound changes in plasma metabolome, ii) reduced hydroxymethylglutaryl-CoA synthase upregulation, and mitofusin 2 downregulation, iii) abrogation of LCT-induced mitochondrial enlargement, and iv) enhanced FAO profile. Contrary to literature, mitochondrial biogenesis was unaffected by KDs. We propose that the observed tissue remodeling is caused by the accumulation of 4-hydroxy-2-nonenal protein adducts, despite an inconspicuous nuclear factor (erythroid-derived 2)-like 2 pathway.

**Conclusion:** We conclude that regardless of the generally favorable effects of MCTs, they cannot inhibit 4-hydroxy-2-nonenal adduct formation and fibrotic tissue formation in this setting. Furthermore, we support the burgeoning concern about the effect of KDs on the cardiac safety profile.



**Keywords** Collagen deposition; Uncoupling protein 3; Dietary therapeutics; Heart diseases; Low carbohydrate diets; 4-HNE

### SIGNIFICANCE STATEMENT

The recent drive to apply dietary measures to fight cardiac disease and risk factors requires a thorough examination and reevaluation of respective animal models. We show strong evidence that rodent models differ in their response towards KD from each other, fatty acid content or ketogenic ratio are secondary for fibrosis induction, and previous data has to be carefully reevaluated. Because we observed cardiac remodeling already after eight weeks, we strongly advise that KD interventions in preclinical studies be reduced to a shorter duration to allow for laboratory versus practice comparisons.

## 1. INTRODUCTION

Cardiovascular diseases (CVDs) are the leading cause of deaths worldwide (WHO 2022). Heart failure is the clinical manifestation of various forms of CVD and is characterized by the accumulation of extracellular matrix proteins (fibrotic tissue formation) and decreased ventricular compliance [1]. In heart failure, proteins of the fatty acid oxidation (FAO) pathway are downregulated, and the myocardium loses the ability to upregulate FAO upon increased fatty acids (FA) supply [2–4]. The deleterious outcome of derangements in FAO is not surprising as recent data in humans shows that ~85% of cardiac ATP

[1]Institute of Physiology, Pathophysiology and Biophysics, University of Veterinary Medicine, Vienna, Austria [2]Department of Pathology, Medical University of Vienna, Vienna, Austria [3]Leibniz Institute for Food Systems Biology at the Technical University of Munich, Munich, Germany [4]Department of Nutritional Sciences, University of Vienna, Vienna, Austria [5]Department of Physiological Chemistry, Faculty of Chemistry, University of Vienna, Vienna, Austria [6]Chair for Nutritional Systems Biology, Technical University Munich, Freising, Germany [7]Institute of Morphology, University of Veterinary Medicine, Vienna, Austria [8]Research Program for Receptor Biochemistry and Tumor Metabolism, Department of Pediatrics, Paracelsus Medical University, Salzburg, Austria

*Corresponding author.

**Corresponding author.

E-mails: felix.sternberg@vetmeduni.ac.at (F. Sternberg), christina.sternberg@meduniwien.ac.at (C. Sternberg), a.dunkel.leibniz-lsb@tum.de (A. Dunkel), taraneh.beikbaghban@vetmeduni.ac.at (T. Beikbaghban), andras.gregor@univie.ac.at (A. Gregor), aleksanderszarzynski@hotmail.com (A. Szarzynski), v.somoza.leibniz-lsb@tum.de (V. Somoza), Ingrid.walter@vetmeduni.ac.at (I. Walter), kalina.duszka@univie.ac.at (K. Duszka), b.kofler@salk.at (B. Kofler), elena.pohl@vetmeduni.ac.at (E.E. Pohl).

Received December 5, 2022 • Revision received March 9, 2023 • Accepted March 14, 2023 • Available online 21 March 2023

https://doi.org/10.1016/j.molmet.2023.101711

  

production derives from FA, ~6.4% from ketone bodies (KBs, e.g. beta-hydroxy-butyrate [β-OHB]), ~4.8% from amino acids, and ~2.8% from lactate [5].

Ketogenic diets (KDs) have been used for decades to treat epilepsy in children and have been recently evaluated as safe in an epileptic treatment setting [6,7]. Furthermore, KDs are used for patients with diabetes and Parkinson's disease, and are the focus of adjuvant cancer therapy [8–11]. Ketogenic diets reduce insulin and glucose signaling, and an increase in β-OHB mediates positive effects on health span and life span in rodents [12,13]. Beta-hydroxy-butyrate suppresses oxidative stress, induces mitochondrial adaption and resilience, and acts anti-inflammatorily [14–18]. Consequently, an interest in applying KDs as a therapeutic intervention to treat heart disease is rapidly emerging since KDs with a high-fat and low-carbohydrate content can improve CVD by, for example, providing FA for FAO, increasing insulin sensitivity, normalizing body weight as well as lipoprotein levels in people without [14–16,19] and with type 2 diabetes [20]. However, it is noteworthy that KD led to hepatic insulin resistance in mice [21] highlighting the significance of the correct understanding of the models in place.

Ketogenic diets can be composed of long-chain triglycerides (LCTs; FA $\geq$ 12 carbon chains [C12]) and medium-chain triglycerides (MCTs) with FA $\leq$ C10. As KDs are composed mainly of fat, the resulting increase in available FA might be beneficial for organs that rely mainly on FAO such as the heart. In humans, MCTs induce higher β-OHB plasma levels than LCTs. In murine models, they exert stronger anti-inflammatory effects in inflammatory models of the intestine, gut, and obesity. Ketogenic diets also ameliorate insulin resistance and reduce signs of cardiomyocyte aging [22–25]. Importantly, MCT-derived FA octanoate (C8) is beneficial in murine reperfusion injury due to a slowdown of electron transport, reduced oxidative stress, and increased signs of long-chain FA β-oxidation [26].

After increased FA uptake, healthy cardiac tissue responds by upregulating peroxisome proliferator-activated receptor-γ1 (PPARγ1), mitochondrial uncoupling protein 3 (UCP3), carnitine-acylcarnitine transferases 1 and 2 (CPT1, CPT2), and carnitine-acylcarnitine translocase (SLC25A20) [4,27–30]. The levels of FA-carnitine species, produced by mitochondrial CPT1, are an important readout for the metabolic state of the heart, and plasma levels of acyl-carnitines reflect the cardiac acyl-carnitine profile levels at least in rodents [31]. Cytoplasmic FAs are activated, esterified onto a glycerol backbone, and incorporated into lipid droplets (LDs). Because lipid accumulation in the heart is a common cause of heart disease [32], LD storage is crucial to protect the heart from excessive FA, which in the case of polyunsaturated (ω-6) FA can get oxidized by e.g. hydroxyl radicals resulting in highly reactive 4-hydroxy-2-nonenal (4-HNE) aldehyde species, which covalently bind proteins [33] and alter mitochondrial protein activity [34,35]. 4-HNE protein adducts show reduced activity, resulting in cellular dysfunction and tissue damage. Of note, 4-HNE levels themselves directly correlate with several cardiovascular diseases [36]. In the heart, the LD-coating protein, perilipin 5 (Plin5), regulates lipases that supply FA from LDs for mitochondrial uptake [37]. Cardiac-specific Plin5 overexpression leads to lipid droplet accumulation and cardiac dysfunction in mice [38].

Despite many reported positive effects of KDs, we recently linked MCT-rich KDs to the inflammatory skin disease, psoriasis, which is a common comorbidity of CVD [39]. LCT-rich KDs have been shown to induce cardiac fibrosis via activation of fibroblasts in spontaneously hypertensive rats, but not in healthy control rats, after four weeks [40]. Other research groups reported reduced mitochondrial biogenesis and subsequent cardiomyocyte death in rats after 16 weeks of KD feeding [41]. Further reports made the suppression of regulatory T-cell function and fibroblast activation in obese mice responsible for cardiac fibrosis after 12 weeks [42].

Given our new understanding of the adverse effects of LCT-KDs on cardiac tissue, we hypothesize that the composition and duration of KD might be crucial for the development of fibrosis. Therefore, we investigated the effects of MCT supplementation of LCT diets on murine cardiac tissue and the effect on cardiac FAO–related transcription and translation in healthy adult male mice. For the application of KD we chose an intermediate time frame of eight weeks and assessed histological evidence for heart fibrosis, markers of FAO, the plasma metabolome, LD population, molecular targets of cardiac integrity, mitochondrial biogenesis as well as cardiomyocyte ultrastructure in male C57/BL6NRJ mice.

## 2. MATERIALS AND METHODS

### 2.1. Experimental animal model

All animal experiments were approved by the Austrian national authority according to §§ 26ff. of the Animal Experiments Act, Tierversuchsgesetz 2012-TVG 2012 (BMWFW-66.006/0008-V/3b/2018). All procedures were in alignment with the directive 2010/63/EU of the European Parliament on the protection of animals used for scientific purposes. Male C57/BL6NRJ mice were housed under a 12 h/12 h dark–light cycle at 23 °C. For the first twelve weeks after birth, the mice were kept under the same dietary conditions. Afterward, they were separated into groups of five and three animals for housing and put on different diets over a period of eight weeks (Supplementary Table 1, Figure 1). The animals were sacrificed by inhalation of an overdose of Sevoflurane (Minrad Inc., Bethlehem, PA, USA). To control for levels of ketosis, β-OHB levels were assessed in plasma using a colorimetric enzymatic kit (MAK041-1 KT; Sigma–Aldrich, Vienna, Austria) following the manufacturer's instructions. Mice under CR were fed once a day with 80% of the calories of a SD-fed mouse for the last 2 weeks as reported in [43]. Water was provided *ad libitum* in all groups.

### 2.2. RNA and protein isolation

RNA was isolated using a guanidine isothiocyanate/phenol method as described previously [39,44]. Protein was precipitated out of the organic phase using 750 µl isopropanol for 10 min at room temperature (RT). Subsequently, samples were centrifuged for 10 min at 12,000 × *g* at 4 °C. The supernatant was discarded, and the pellet was washed three times with 1 mL 0.3 M guanidine hydrochloride (GdmCl; Sigma–Aldrich) in 95% ethanol using an incubation of 20 min at RT before centrifugation and changing the wash solution. After the third wash, the washing solution was removed completely, and the pellet was vortexed in >99.9% ethanol followed by another 20 min incubation at RT to dissolve the rest of the GdmCl out of the pellet. The pellets were stored in >99.9% ethanol at 4 °C until solubilization. Proteins were solubilized with 1% SDS solution (in phosphate buffered saline; Sigma–Aldrich) after drying samples fully in a thermomixer (50 °C, 400 rpm) with open lids. After breaking the pellet with a needle, it was incubated for 2 min at 50 °C followed by 8 min at 60 °C. Then, the protein solution was sonicated three times for 3 s on ice, incubated for half an hour on ice, and centrifuged before collecting the supernatant for storage at −80 °C. We additionally, performed protein isolation using a lysis buffer consisting of radioimmunoprecipitation (RIPA) buffer and a protease inhibitor cocktail (Sigma–Aldrich), as previously published [45].

 

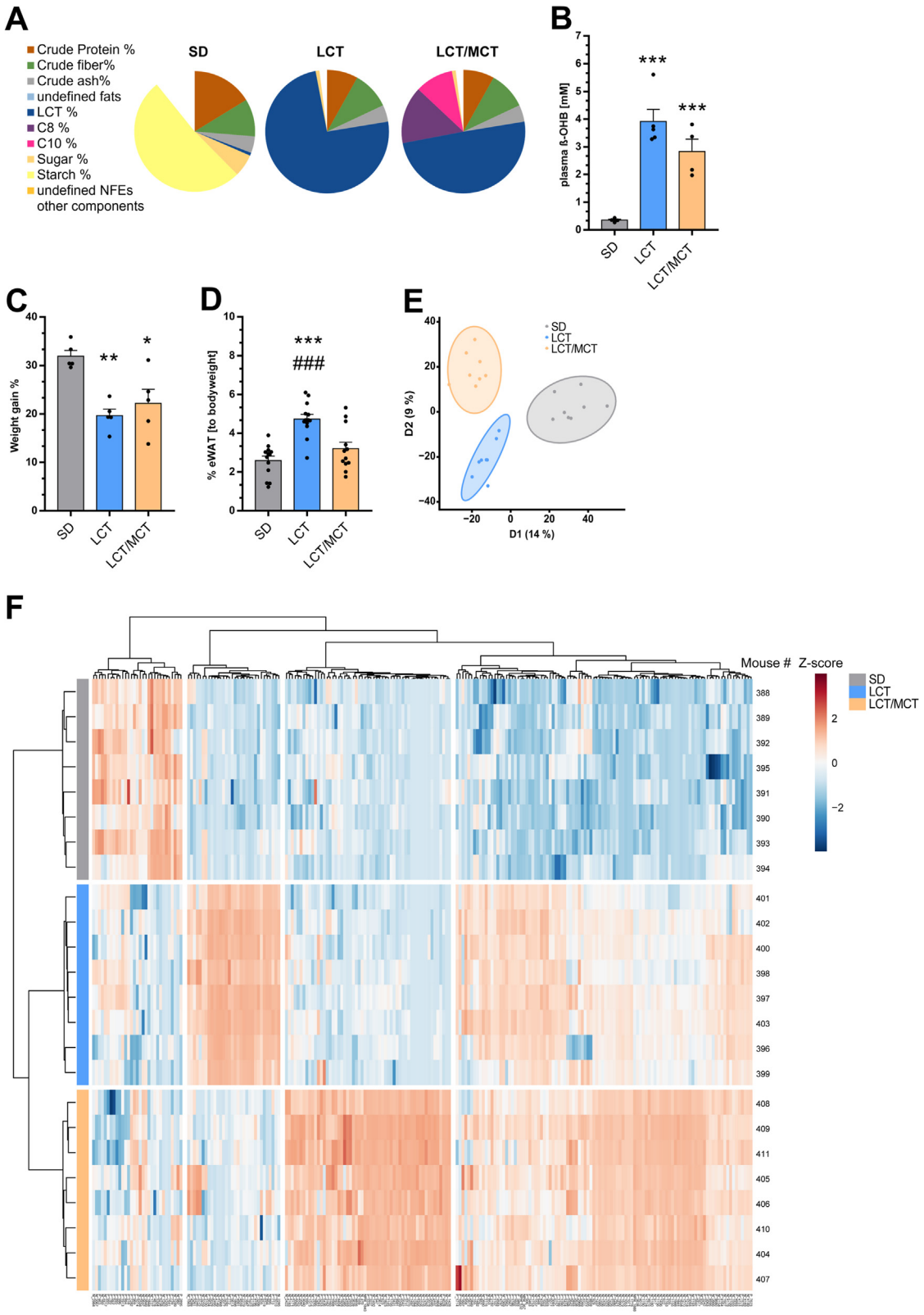


**Figure 1: KDs are not obesogenic and addition of MCT reduces LCT mediated fat depot increase in mice and alters plasma metabolome profile.** (**A**) Graphical presentation of diet compositions, (**B**) β-OHB plasma levels, (**C**) body weight gain %, (**D**) eWAT depots, (**E**) Score plot of Partial Least Squares – Discriminant Analysis of untargeted plasma metabolomics data and (**F**) Heatmap of selected mouse plasma metabolites with high diet-specific differences based on volcanoplot separation (Figures. S1A–C). Values are mean ± SEM from n = 4–5 (B–C), n = 8–13 (D–F) individual mice per group. $^{*}P < 0.05$, $^{**}P < 0.01$, $^{***}P < 0.001$ versus SD, # versus KD. Statistical significance was assessed using one-way analysis of variance. β-OHB, beta-hydroxy-butyrate; eWAT, epididymal white adipose tissue; LCT, long-chain triglycerides; MCT, medium-chain triglycerides; SD, standard diet; SEM, standard error of the mean.

 

### 2.3. cDNA synthesis and gene expression analysis

Reverse transcription and quantitative reverse transcription (qRT)-PCR were performed as previously described [39,44]. In brief, RNA integrity was verified on a TapeStation4200 System, an automated electrophoresis tool for RNA quality control (Agilent, Vienna, Austria) and showed mRNA integrity values $> 8$. For cDNA synthesis, 2 μg of RNA was used and digested with DNase I (Thermo Fisher Scientific, Vienna, Austria). Reverse transcription was performed using a High-Capacity cDNA Reverse Transcription Kit (Applied Biosystems, Vienna, Austria), random primers, and RiboLock RNase inhibitor (Thermo Fisher Scientific). Primers for qRT-PCR were designed using NCBI primer-blast. Primers were designed to span exon—exon junctions and PCR product size was kept in the range of 80—150 bp to ensure high primer efficiency, which was checked via the serial dilution of cDNA. Amplicon sizes were checked on polyacrylamide gels. Primer sequences are given in Supplementary Table 2. Quantitative reverse transcription-PCR was performed on a qTower384 real-time PCR system (Analytik Jena, Jena, Germany) using Luna (New England Biolabs, Frankfurt am Main, Germany) master mix. Plates were loaded in triplicates by an epMotion 5075 (Eppendorf, Vienna, Austria) pipetting robot using 1:1 diluted cDNA, with a 62 °C annealing temperature. Beta-actin was used as a housekeeping gene. Additionally, we evaluated the stability of β-actin expression toward transcripts of ribosomal protein L4.

### 2.4. Immunoblotting and antibodies

In the supplementary information, uncropped immunoblots are shown. Western blotting was performed as previously described [45]. In brief, 20 μg of protein diluted in reducing protein loading dye was loaded onto 0.75-mm thick SDS polyacrylamide gels, consisting of 3.75% polyacrylamide stacking and 12% polyacrylamide separating gels. A mini-PROTEAN® Tetra handcast system was used to cast and run the polyacrylamide gels. As a positive control for UCP3 immunoblots, 5 μg of recombinant UCP3 was loaded onto each gel [46]. Following electrophoresis, gels were transferred to polyvinylidene fluoride membranes (Amersham Hybond 0.45 μm; GE Healthcare, Boston, MA, USA) for 1 h at 14 V using a semi-dry blotter (Peqlab, Erlangen, Germany) and methanol-containing blotting buffer. The membranes were then stained with Ponceau S solution to verify successful blotting and to visualize total protein. After blocking the membranes for 1 h in 2% bovine serum albumin (BSA; Sigma—Aldrich) blocking solution at RT, they were incubated with primary antibodies overnight at 4 °C. All primary and secondary antibodies were diluted with 2% BSA block solution. Details on antibodies used are given in Supplementary Table 3.

Semi-quantitative analysis of western blots was done using Software VisionWorks 8.20 (Analytik Jena). The intensity of the target protein ($I_{TP}$) bands representing protein expression was related to the band intensities of mitochondrial (OGDH or TOM20) or cytoplasmic (α-tubulin) markers ($I_{HK}$) as a cytoplasmic normalization protein ($I_{rel} = I_{TP}/I_{HK}$ = relative protein amount). These ratios were normalized membrane internally to at least 3 SD-fed mouse tissues. Every sample was electrophoresed and transferred to at least two different membranes; the average of normalized values was calculated and used for statistical analysis.

### 2.5. Ultrastructure analysis

The apex region of the left ventricle and mid-myocardium was used. Tissue was fixed in 3% buffered glutaraldehyde (pH 7.4; Merck, Darmstadt, Germany) and washed with 0.1 M Sorensen phosphate buffer at pH 7.4. All samples were subsequently postfixed in 1% osmium tetroxide (Electron Microscopy Sciences, Hatfield, PA, USA) followed by dehydration in a series of ethanol dilutions (70, 80, 96, and 100%), embedded in Epon resin (Sigma—Aldrich) and polymerized for 48 h at 60 °C. Semi-thin sections (0.8 μm) were stained with toluidine blue and 2 μm sections with *p*-phenylenediamine (PPD, Sigma) to demonstrate LDs. Ultra-thin sections (70 nm) were mounted on copper grids (Science Services, Munich, Germany) and stained with uranyl acetate and lead citrate (Sigma). Transmission electron micrographs were made with EM900 (Zeiss, Oberkochen, Germany). Border regions of the left ventricle were assessed ensuring well-preserved mitochondria due to fast fixative permeation. Using ImageJ (NIH, Bethesda, MA, USA) we manually analyzed approximately 400 mitochondria in at least three independent transmission electron microscopy (TEM) micrographs per mouse. The individual mitochondrial perimeters and whole micrograph areas were measured. From each PPD-stained heart tissue, images of two individual sections were taken with 20 × magnification (Axioscope; Zeiss, Vienna, Austria). This region was subclustered into 3—4 images with 40 × magnification, which were used for analysis. Lipid droplets visualized by PPD were counted in the same regions as mitochondria. Approximately 1000 LD counts per section and per mouse were recorded, and the total area assessed was used to normalize LD counts. The individual LD perimeters were analyzed in the same way the mitochondrial perimeter analysis was done on the exact same TEM micrographs.

### 2.6. Histology

Transversal cut heart (central region) was used. Samples were fixed in 4% paraformaldehyde in 0.1 M phosphate buffer and embedded in paraffin. Heart sections (5 μm) were cut with a rotary microtome and fixed on a microscope glass slide. Samples were deparaffinized in a descending alcohol series, starting with xylene and ending in $dH_2O$.

For picrosirius red staining, sections were incubated in 0.1% picrosirius red solution (Sirius red F3B, Sigma—Aldrich) in 1.3% aqueous picric acid solution (Sigma—Aldrich) for 60 min. Afterward, specimens were washed in acidified water and dried, followed by washing in an ascending alcohol series starting with isopropanol and ending in xylene. During the washing process, the samples were protected from direct light irradiation. Stained samples were covered with DePeX (Merck, Darmstadt, Germany) and kept in the dark.

For Masson trichrome staining, sections were incubated in Bouin's solution (Sigma—Aldrich) overnight in a light-protected humidity chamber. Afterward, the samples were incubated in Weigert's iron hematoxylin solution (Sigma—Aldrich) for 5 min, briefly washed in $H_2O$ for 10 min, placed in $dH_2O$, and incubated in Masson-Goldner-I solution (Carl Roth, Karlsruhe, Germany) for 5 min. After 5 min, 1% acetic acid solution (Sigma—Aldrich) was added for 30 s; the samples were incubated in Masson-Goldner-II solution (phosphomolybdic acid - orange G; Carl Roth) for 30 min and in Masson-Goldner-III (Anilinblue) solution (Carl Roth) for 6 min. The blue staining solution remained on the samples while 1% acetic acid solution was added for 2 min. Afterward, samples were briefly washed with $dH_2O$, followed by an ascending alcohol series starting with isopropanol and ending in xylene. Stained samples were covered with DPX (Merck). For H&E staining, sections were incubated in Mayer's hemalum solution (Carl Roth) for 4 min and briefly washed in $H_2O$ for 10 min. Samples were then incubated in 1% aqueous eosin (yellowish) for approximately 10 s, followed by an ascending alcohol series starting with 70% EtOH (Sigma—Aldrich) and ending in xylene (Sigma—Aldrich). Stained samples were covered with DPX (Merck).

 

### 2.7. Histological evaluation

Images of each specimen were taken with an Axiocam 503 color microscope camera (Zeiss) using an Axioscope microscope (Zeiss). Quantitative analysis of picrosirius-stained collagen fibers was performed as described previously [47].

From each picrosirius red—stained heart tissue, six images were taken (three of the ventricle, three of the septum) using an objective with 20 × magnification. The images were taken with a polarized light microscope (Axioscope, Zeiss). The birefringence of polarized light is extremely specific for collagen. The quantitative analysis of collagen fibers was performed with images taken by polarized light microscopy using ImageJ (NIH). Each image was analyzed using the same evaluation criteria. To ensure that only fibrotic collagen was counted, we used a subtraction method to remove non-collagen elements, blood vessels, and interstitial space from images. The fiber hue of collagen was obtained, and the number of green, yellow, orange, and red pixels (ordered by ascending thickness) relative to the total number of pixels was calculated to determine the average value for each mouse. Furthermore, the collagen content was calculated as a percentage of the area of each image, which was 1920 × 1460 pixels. For data analysis, thin (green) collagen fibers were taken as these are newly generated fibers.

### 2.8. Untargeted metabolomics

Plasma samples were analyzed as recently shown [43] by UHPLC-TOF-MS/MS using an Exion LC UHPLC system (Sciex, Darmstadt, Germany) connected to a TripleTOF 6600 mass spectrometer (Sciex) via electrospray ionization (ESI) in negative and positive mode. To extend metabolite coverage to short-chain carbonyl compounds, additional derivatization experiments were performed. For derivatization, 40 µl of the plasma extract was mixed with 20 µl of a solution of 3-nitrophenylhydrazine (200 mM; 50:50 v/v; ACN/$H_2O$) and 20 µl of a 120 mM solution of N-(3-dimethylaminopropyl)-N′-ethylcarbodiimide in 6% pyridine (50:50 v/v; ACN/$H_2O$) and reacted for 30 min at 40 °C. Afterwards, the mixture was diluted with ACN/$H_2O$ (200 µl; 50:50 v/v) and used directly for UHPLC-TOF-MS/MS analysis [48—50]. Data analysis of mass spectrometry data was performed using the R programming language for statistical computing (version 4.2.2) with multiple extension packages. Raw mass spectrometry data was converted to the mzML file format using Proteowizard ms convert [51] and subsequently processed using the xcms package (version 3.20.0) [52]. Peak areas of detected features in the individual samples were used for the discriminative analysis of differences between experimental groups by Partial Least Squares—Discriminant Analysis (PLS-DA) (ropls package, version 1.30.0), while statistical analysis for volcano plot visualization was performed using the limma package (version 3.54.2) [53]. Figures used in the manuscript were generated using the ggplot2 package (version 3.4.1).

### 2.9. Statistics

Data of gene and protein expression were analyzed using GraphPad Prism software 7 (GraphPad Software, San Diego, CA, USA). Relative mRNA was calculated using the $2^{-\Delta Ct}$ method, one-way analysis of variance (ANOVA), with a Kruskal—Wallis test for non-parametric data and Dunn's multiple comparisons test was applied. Data from KDs (LCT, LCT/MCT) and fasting experiments (CR) were compared to a standard diet (SD), respectively. Protein expression was analyzed with ordinary one-way ANOVA using Dunnett's multiple comparisons test. Outliers were detected using Grubbs' test; the significance level (alpha) was set to 0.05. Significant differences are indicated as: $*P \leq 0.05$, $**P \leq 0.01$, $***P \leq 0.001$.

## 3. RESULTS

### 3.1. KD feeding is not obesogenic and the addition of MCT results in a distinct plasma metabolome profile

We monitored the body weights of mice throughout the diet treatment and assessed epididymal white adipose tissue (eWAT) depots at the end of the 8-week feeding period to exclude obesity induction, a known cardiac risk factor. The composition of the KD (Figure 1A) was based on our previous studies [8,39,54]. The ketogenic ratio was set to 8:1 (fat vs. carbohydrates and protein), and the diets were classified as standard diet (SD), long-chain triglyceride-based KD (LCT), consisting of mostly C16 and C18 FA, and a mix of 34% medium-chain triglycerides (MCTs) and 66% LCT (LCT/MCT). Medium-chain triglyceride fat was a mix of 60% C8 and 40% C10 oil (Supplementary Table 1). Both LCT and LCT/MCT feeding significantly increased levels of plasma β-OHB compared to the SD (Figure 1B, LCT: 3.92 ± 0.96 mM; LCT/MCT: 2.83 ± 0.89 mM; SD: 0.35 ± 0.06 mM). Long-chain triglyceride and LCT/MCT feeding resulted in a similar body weight gain (Figure 1C). LCT but not LCT/MCT resulted in increased eWAT depots compared to the SD (Figure 1D). Of note, assessment of food intake was not reliable as the consistency of the diets lead to mixing with the embedding material inside the cages.

To validate that MCT addition clearly induces a different metabolic response in mice, we performed untargeted plasma metabolomics. Discriminant analysis of metabolomics data showed clear separation between the groups (Figure 1E), accordingly highly specific metabolite clusters between the diet groups were observed (Figure 1F), clearly indicating different whole body metabolism responses upon addition of LCT and the addition of MCT compared to SD. Metabolites upregulated between the groups are shown in Supplementary File Metabolomics. In alignment with enzymatic β-OHB determination (Figure 1B) metabolomics data mirrored β-OHB ratios between groups (Figure S1D). As expected, both KDs reduced plasma hexose levels significantly (Figure S1E).

### 3.2. Supplementation with MCTs fails to rescue LCT-derived fibrosis but decreases cardiac ketogenesis-related HMGCS expression

To evaluate whether the heart responds to LCT and LCT/MCT diets differently at the molecular level, we analyzed mRNA transcripts of the mitochondrial rate-limiting ketolytic enzyme, succinyl-CoA:3-ketoacid-coenzyme A transferase (*Oxct1*), and the fate-committing enzyme of cardiac ketogenesis, hydroxymethylglutaryl-coenzyme A-synthase (*Hmgcs2*). Long-chain triglyceride and LCT/MCT feeding resulted in a significantly reduced mRNA level of *Oxct1* and a massive (14-fold) increase in *Hmgcs2* mRNA compared to the SD (Figure 2A). This indicates that the heart tries to produce its own β-OHB, as suggested previously [55]. Interestingly, immunoblotting for HMGCS protein showed an increased abundance in samples from LCT compared to LCT/MCT groups, and no quantifiable amount in the SD-fed cohort (Figure 2B—C), levels of OXCT1 protein were similar between groups (Figure 2D—E). We introduced caloric restriction (CR, 80% calories of SD) to exclude energy deficiencies as a reason for KD related effects. Mice on CR lost body weight (14.6 ± 2.6%, n = 8) and eWAT depots were diminished accordingly (Figure S2). The cardiac tissue of these mice showed only a slight (2-fold) increase in *Hmgcs2* mRNA

 

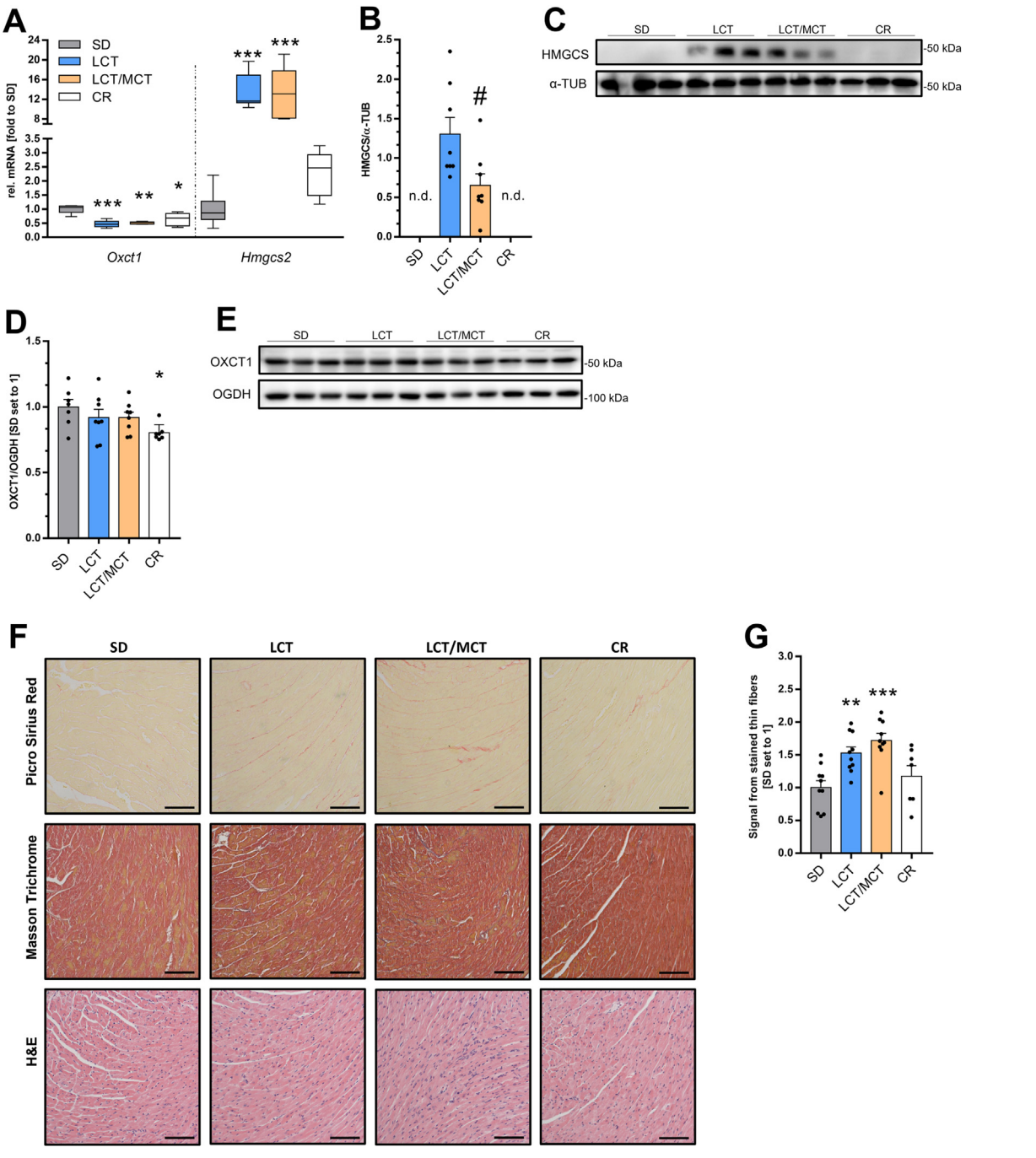


**Figure 2: KDs induce a distinct gene expression pattern and fibrotic tissue formation in mice.** (**A**) Relative mRNA levels of *Oxct1* and *Hmgcs2* in heart sections of SD, LCT, LCT/MCT, CR-fed mice after eight weeks. (**B**–**C**) Quantification and representative immunoblot of HMGCS protein in cardiac tissue samples. α-TUB serves as loading control. (**D-E**) Quantification and representative immunoblot of OXCT1 protein in cardiac tissue samples. OGDH serves as loading control. (**F**) Representative images of picrosirius red (upper row), Masson trichrome (middle row), and H&E (bottom row) stained mouse hearts. Scale bar = 100 μm. Picrosirius red: collagen filaments appear red, muscle fibers and cell cytoplasm appear pale yellow. Masson trichrome: collagen filaments appear blue, muscle fibers and cytoplasm appear red. H&E: nuclei are deep blue, cytoplasm is pink. (**G**) Quantification of collagen fibers stained with picrosirius red in images taken by polarized light microscopy. $^{*}P < 0.05$, $^{**}P < 0.01$, $^{***}P < 0.001$ versus SD, # vs. KD. Statistical significance was assessed using a one-way analysis of variance or non-parametric Kruskal–Wallis test (mRNA). Values are mean ± SEM from, n = 7–8 (A–B) and n = 7–10 (D–G) individual mice per group. α-TUB, alpha-Tubulin; CR, caloric-restricted diet; H&E, hematoxylin and eosin; HMGCS, hydroxymethyl glutaryl-coenzyme A-synthase; KD, ketogenic diet; LCT, long-chain triglycerides; MCT, medium-chain triglycerides; n. d., not detected; OGDH, 2-oxoglutarate dehydrogenase E1; Oxct1, succinyl-CoA:3-ketoacid-coenzyme A transferase; SD, standard diet; SEM, standard error of the mean.

 

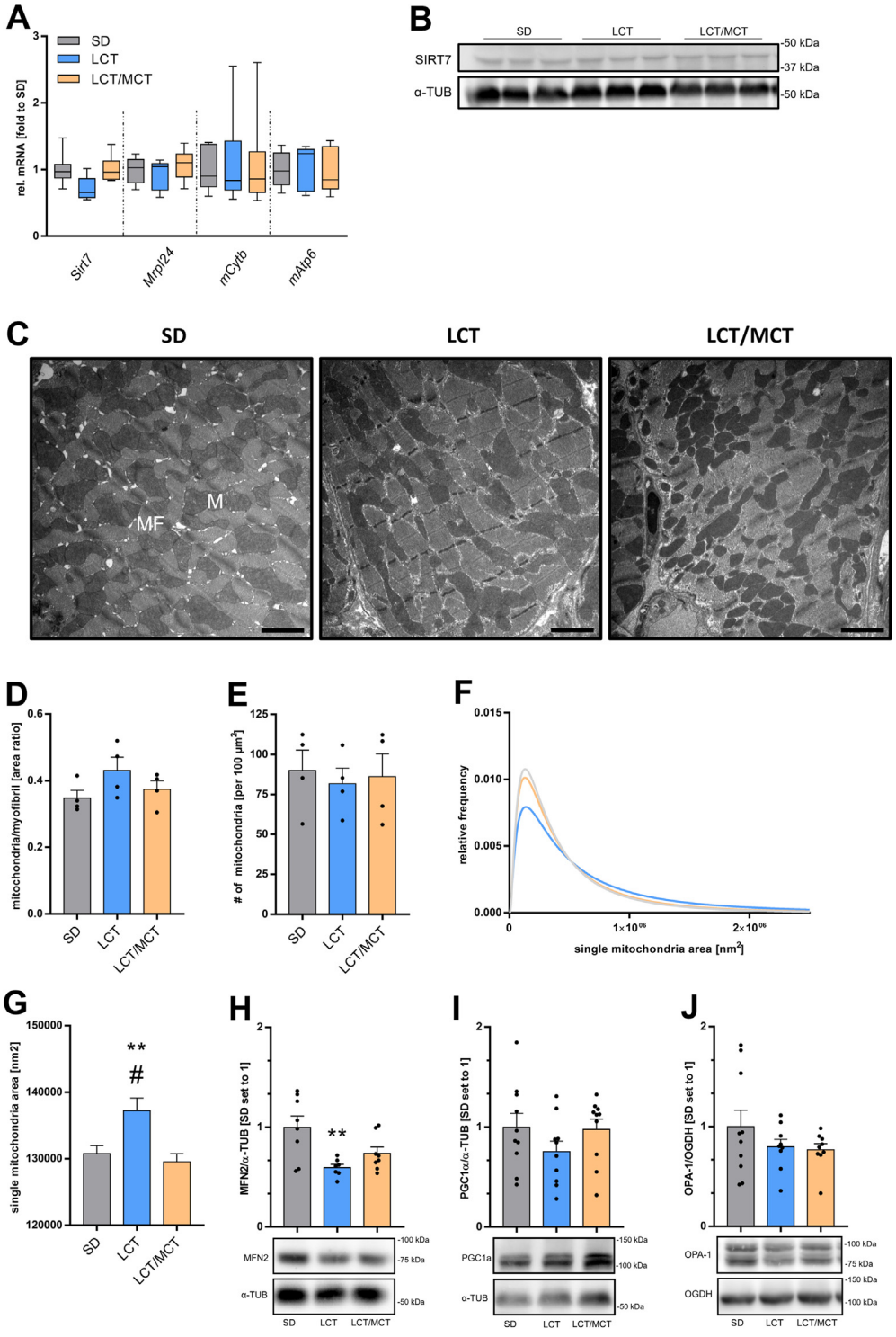


**Figure 3: KDs do not alter cardiac mitochondrial biogenesis, and MCT addition restores LCT-KD mediated mitochondrial size and MFN2 alterations.** (**A**) Relative mRNA levels of *Sirt7*, *Mrpl24*, *mCytb*, and *mAtp6* in heart sections of SD-, LCT-, or LCT/MCT-fed mice after eight weeks. (**B**) Representative immunoblot of SIRT7 protein in cardiac tissue. (**C**) Representative TEM micrographs of cardiac tissue which were used for surface ratio and mitochondrial size analysis. M: exemplary mitochondria, MF: myofibrils; scale bar = 2 µm. (**D**) Mitochondria to myofibril surface ratio, and (**E**) amounts. (**F**) Nonlinear Log (Gaussian) fit ($R^2 \geq 0.85$) of mitochondrial size based on SD: 1891, LCT: 1868 and LCT/MCT: 2669 single mitochondria visualized by TEM and (**G**) resulting best-fit center values with standard error of mitochondrial size ($nm^2$). (**H**) Quantification and representative immunoblots of MFN2, (**I**) PGC1-α and (**J**) OPA-1. $^{**}P < 0.01$ versus SD, # versus KD. Statistical significance was assessed using a one-way analysis of variance or non-parametric Kruskal–Wallis test (mRNA). Values represent mean ± SEM from n = 7–10 (A, H-J) or n = 4 (D–E) individual mice per group. α-Tub and OGDH served as protein loading controls. LCT, long-chain triglyceride; M, Mitochondria; *mAtp6*, mitochondrially encoded ATP synthase membrane subunit 6; MCT, medium-chain triglycerides; *mCytb*, mitochondrially encoded cytochrome B; MF, myofibrils; *Mrpl24*, nuclear-encoded mitochondrial ribosome protein L24; MFN2, mitofusin 2; OGDH, 2-oxoglutarate dehydrogenase E1; OPA-1, optic atrophy 1; PGC1-α, peroxisome proliferator-activated receptor gamma coactivator 1-alpha; SD, standard diet; SEM, standard error of the mean; SIRT7, Sirtuin 7; α-TUB, α-tubulin; TEM, transmission electron microscopy.

 

compared to SD-fed mice which did not translate in detectable levels of HMGCS protein (Figure 2B—C), but mRNA levels of *Oxct1* were significantly downregulated (Figure 2A) together with OXCT1 protein (Figure 2D—E).

Because few previous reports linked LCT-KD to fibrosis induction [40—42], we first assessed tissue integrity by picrosirius red and Masson trichrome staining (Figure 2F, upper and middle panel). Quantification of picrosirius red via polarized light microscopy revealed a significant increase in collagen fibers in the cardiac tissues of LCT- and LCT/MCT-fed mice compared to SD-fed mice (Figure 2G). We excluded increased immune cell infiltration as the cause of fibrosis by qualitative inspection of hematoxylin and eosin-stained nuclei (Figure 2F, lower panel) which did not show any apparent differences between the groups. No significant changes in the amount of collagen fibers in CR hearts compared to those of animals on an SD were observed (Figure 2F—G).

### 3.3. Mitochondrial biogenesis is unaffected by KDs

An LCT-KD was reported to increase sirtuin 7 mRNA levels (*Sirt7*/SIRT7) and reduce mitochondrial ribosome protein L24 transcripts (*Mrpl24*) resulting in the impairment of mitochondrial biogenesis and cardiac fibrosis in rats [41]. Interestingly, despite impaired mitochondrial biogenesis, cardiomyocytes isolated from LCT-KD- and SD-fed rats had similar basal and ATP-driven mitochondrial oxygen consumption rates. Accordingly, we re-evaluated the suggested pathways. Long-chain triglyceride and LCT/MCT-fed mice showed similar transcript levels of *Sirt7* and *Mrpl24* as SD-fed mice (Figure 3A). Transcripts of mitochondrially-encoded cytochrome B (*mCytb*) and ATP synthase membrane subunit 6 (*mATP6*), as indicators of mitochondrial biogenesis, were not changed upon dietary intervention (Figure 3A). These data are in line with stable SIRT7 protein levels (Figure 3B). Transcript levels of *Sirt7*, *Mrpl24*, *mCytb* and *mAtp6* in CR-fed mice were on par with SD (Figure S3). Furthermore, we did not detect any changes in the ratio of mitochondria to myofibrils between the mouse groups upon KD feeding (Figure 3C—D), or numbers of mitochondria between the diet groups (Figure 3E). Interestingly we observed a shift in mean mitochondrial size upon LCT feeding compared to SD which was abrogated upon MCT addition (Figure 3F—G). Previous reports connected cardiac mitochondrial enlargement, impaired mitophagy, and cardiomyopathy to lack of mitofusin 2 (MFN2) [56]. We detected significantly lower MFN2 protein levels in the LCT group (Figure 3H). Protein levels of peroxisome proliferator-activated receptor gamma coactivator 1-alpha (PGC1-$\alpha$), which positively correlates to mitochondrial biogenesis [57] and is reduced in the failing heart [58], were unaffected in our study (Figure 3I). Mitochondrial optic atrophy 1 (OPA-1) protein, which is involved in mitochondrial morphology, cytoarchitecture, and heart function [59,60], was not altered between the groups (Figure 3J). We previously observed a strong increase in mitochondrial cristae density upon functional maturation in the mouse heart [45]. Accordingly, we scored mitochondrial cristae density but did not reveal any significant differences between groups (Figure S4). Of note, this analysis is limited due to the 2D nature of the micrographs and mitochondrial heterogeneity. We concluded that mitochondrial biogenesis was not affected in the hearts of LCT- and LCT/MCT-fed mice. However, upon LCT-feeding we depicted mitochondrial enlargement together with lower levels of MFN2, both effects were dampened upon MCT supplementation.

### 3.4. MCT addition increased LCT-mediated upregulation of cardiac FAO markers, plasma acetylcarnitine and palmitoylcarnitine levels

Because a failure of mitochondrial biogenesis cannot explain cardiac fibrosis upon KD feeding, we hypothesized that alterations of portions of the FAO pathway or lipid homeostasis may be responsible. We analyzed transcripts of mitochondrial FA transport proteins (FA $\geq$ 12C), *Cpt1a*, *Slc25a20*, and *Cpt2*, the FA sensor, *Ppar$\gamma$1* [4], and an FAO biomarker in the heart, *Ucp3*/UCP3 [29,45]. Interestingly, LCT-based KD induced only the gene expression of *Cpt1a* and *Ucp3*, whereas LCT/MCT feeding increased *Cpt1a*, *Cpt2*, *Ucp3*, and *Ppar$\gamma$1* (Figure 4A). This is in line with significantly elevated protein levels of UCP3 upon LCT and LCT/MCT feeding (Figure 4B—C). LCT/MCT tended to increase UCP3 protein levels more strongly compared to LCT feeding ($P = 0.06$). Both KDs significantly elevated SLC25A20 protein levels (Figure 4D). In line with, the observed molecular changes, levels of free plasma carnitine dropped upon KD feeding (Figure 4E, left panel). Strikingly, the addition of MCT to KD significantly elevated levels of carnitine derivates such as acetylcarnitine and palmitoylcarnitine (Figure 4E, middle and right panel). CR-fed mice did not show any upregulation of *Cpt1a* or *Ucp3*/UCP3 (Figures. S5A—C), accordingly, we exclude reduced energy intake as the trigger of the observed molecular changes.

The quantification of cardiac LD numbers revealed no difference between LCT-, LCT/MCT-, and SD-fed mice (Figure 4F, upper panel, 4G). However, given the changes observed upon plasma metabolome profiling (Figure 1F) and a tendency towards increased C16:0 species in the plasma of both KD-fed cohorts (Figure 4H), we took a closer look at LD depots in the cardiac tissue. Indeed, analysis of heart ultrastructure showed a significant increase in LD size upon LCT- and LCT/MCT feeding (Figure 4F, lower panel, 4I-J). In accordance with LD data, the LD-coating protein and regulator of lipolysis, PLIN5, was 2.1-fold higher in LCT, and 2.5-fold in LCT/MCT-fed mice compared to SD (Figure 4K). In summary, the addition of MCT results in an enhanced cardiac FAO-signature, reflected in the increased plasma abundance of CPT1-derived carnitine-FA species.

### 3.5. Cardiac tissue of LCT and LCT/MCT fed mice revealed an inconspicuous NRF2 pathway but the accumulation of 4-HNE protein adducts

Elevated mitochondrial activity increases ROS and end products such as 4-HNE, both strongly connected to cardiac fibrotic tissue formation [61] and CVD risk [36]. ROS and 4-HNE activate the nuclear factor (erythroid-derived 2)-like 2 (NRF2) pathway to mount an adaptive response [62—64]. In line, KD induced a rise in mitochondrial $H_2O_2$ and 4-HNE levels but finally decreased $H_2O_2$, and normalized 4-HNE levels via constantly elevated NRF2 and heme oxygenase-1 (HO-1) after three weeks of feeding in mice [65].

LCT-KD feeding showed a slight but significant reduction in cardiac NRF2 protein levels, MCT supplementation abolished this effect (Figure 5A). NRF2 target HO-1, induced ubiquitously in response to oxidative stress [66—69], was not affected by KDs (Figure 5B). Interestingly, stable HO-1 levels were recently shown to protect from specific types of myocardial infarction [70]. Stable mitochondrial SIRT3 protein levels are key in the regulation of mitochondrial ROS production [71—73], SIRT3 was unaffected by KD feeding (Figure 5C). In line, *Sod1* mRNA levels, a highly effective cytoplasmic anti-ROS scavenging protein, were similarly expressed between the groups (Figure 5D). In

 

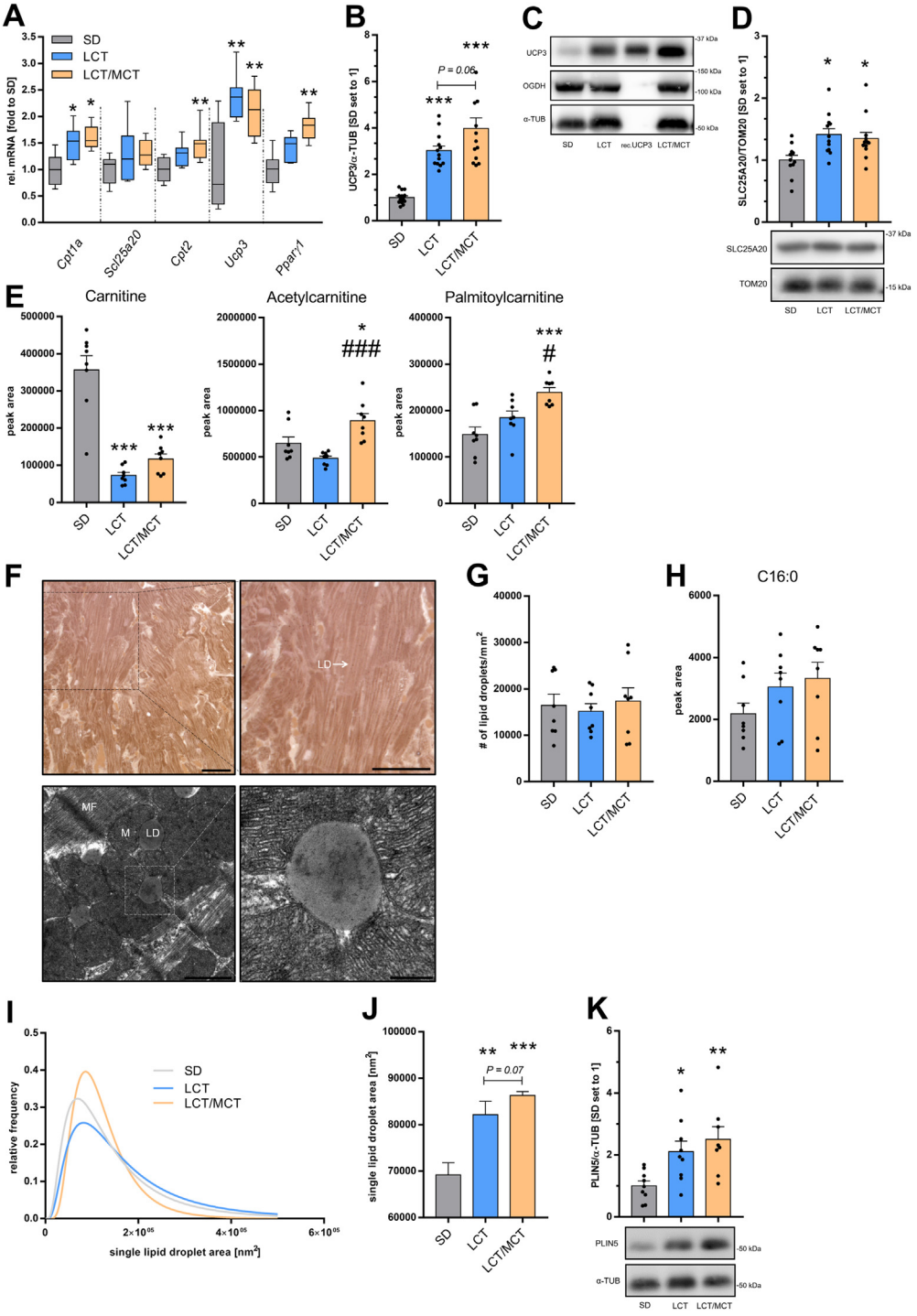


**Figure 4: MCT addition to LCT-KD enhances transcriptional and translation responses towards FA and production of plasma carnitine species.** (**A**) Relative mRNA levels of *Cpt1a*, *Slc25a20*, *Cpt2*, *Ucp3*, and *Pparγ1*, in heart sections of mice fed SD, LCT, or LCT/MCT diets for eight weeks. (**B**) Quantification and (**C**) representative immunoblots of UCP3, and (**D**) SLC25A20 protein. (**E, H**) Individual plasma analyte peak areas from untargeted metabolomics data set of mice fed SD, LCT and LCT/MCT for eight-weeks. (**F**, upper panel) Representative image of PPD-stained LDs (white arrow) in cardiac tissue. Scale bar = 40 μm. (**F**, lower panel) Representative TEM micrograph of cardiac LDs with adjacent mitochondria. Scale bar upper panel = 1 μm, lower panel = 0.2 μm. (**G**) Quantification of LDs in heart tissue of mice fed different diets. (**I**) Nonlinear Log (Gaussian) fit ($R^2 \geq 0.93$) of LD size based on SD: 80, LCT: 80 and LCT/MCT: 82 single LDs visualized by TEM and (**J**) resulting best-fit center values with standard error of LD size ($nm^2$). (**K**) Quantification and representative immunoblot of PLIN5 protein. Values represent mean ± SEM from, n = 7–13 (A-E, H, K), or n = 4 (G-H, J) individual mice per group. $^*P < 0.05$, $^{**}P < 0.01$, $^{***}P < 0.001$ versus SD, # versus KD. Statistical significance was assessed using a one-way analysis of variance or a non-parametric Kruskal–Wallis test (mRNA). α-Tub and TOM20 served as protein loading controls. *Cpt1a*, carnitine palmitoyltransferase 1a; *Cpt2*, carnitine palmitoyltransferase 2; LCT, long-chain triglycerides; LD, lipid droplet; M, mitochondria; MCT, medium-chain triglycerides; MF, myofibrils; OGDH, 2-oxoglutarate dehydrogenase E1; PLIN5, perilipin 5; *Pparγ1*, peroxisome proliferator-activated receptor gamma 1; PPD, *p*-phenylenediamine; recUCP3, recombinant uncoupling protein 3; SD, standard diet; *Slc25a20*, solute carrier 25a20; SEM, standard error of the mean; TEM, transmission electron microscopy; TOM20, mitochondrial import receptor subunit TOM20; α-TUB, α-tubulin; *Ucp3*, uncoupling protein 3.

 

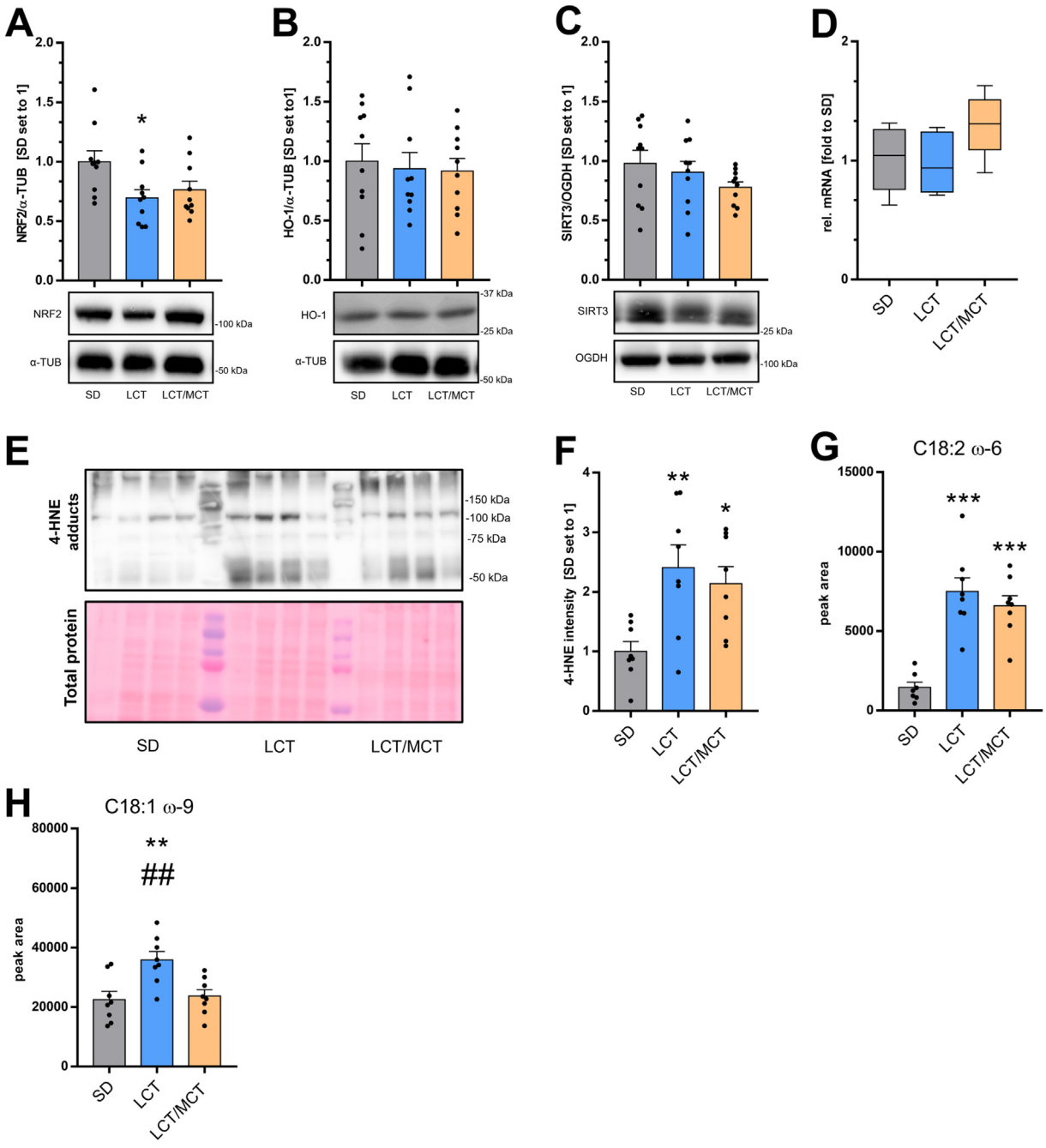


**Figure 5: LCT-KD reduces levels of the oxidative stress sensor NRF2, both diets maintain steady levels of HO-1, SIRT3, and *Sod1* but increase 4-HNE protein adducts in the heart.** (**A**) Quantification and representative immunoblot of NRF2, (**B**) HO-1, and (**C**) SIRT3 proteins in cardiac tissue. α-Tub and OGDH served as loading control. (**D**) Relative mRNA levels of *Sod1* in heart sections of mice fed SD, LCT, or LCT/MCT. (**E**) 4-HNE immunoblot and Ponceau S-stained total protein of cardiac tissue from mice fed SD, LCT, or LCT/MCT diets and (**F**) quantification. (**G-H**) Individual plasma analyte peak areas from the untargeted metabolomics data set of mice fed SD, LCT and LCT/MCT for eight-weeks. Statistical significance was assessed using a one-way analysis of variance or a non-parametric Kruskal—Wallis test (mRNA). Values are mean ± SEM, n = 8—10 mice per group. $^{*}P < 0.05$ versus SD, # versus KD. HO-1, heme oxygenase-1; LCT, long-chain triglycerides; MCT, medium-chain triglycerides; NRF2, nuclear factor-like factor 2; OGDH, 2-oxoglutarate dehydrogenase E1; SIRT3, sirtuin 3; *Sod1*, superoxide dismutase 1; SD, standard diet; α-TUB, α-tubulin; 4-HNE, 4-hydroxy-2-nonenal.

contrast, we observed a strong increase of 4-HNE protein adducts in the LCT and LCT/MCT groups (Figure 5E—F and Figure S6). Plasma analysis revealed elevated 4-HNE precursors C18:2 ω-6 upon KD feeding (Figure 5G). Other moieties such as C18:1 ω-9, was elevated only by LCT feeding (Figure 5H). We exclude an active NRF2 adaptive response in LCT and LCT/MCT fed mouse hearts but revealed elevated 4-HNE protein adducts. We conclude that despite normal ROS, cardiac tissue ω-6 FA availability results in low but constant 4-HNE production and the accumulation of 4-HNE protein adducts, leading to disrupted intracellular signaling and the observed fibrotic remodeling.

 

## 4. DISCUSSION

In the current study, we found that KDs composed of LCT and a mix of LCT and MCT (8:1 ketogenic ratio) induced an increase in collagen fiber content, LD size, carnitine and FA-profile, Plin5, and 4-HNE adduct levels, in the heart of young male C57BL6/N mice after eight weeks. Furthermore, we detected MCT-dependent effects on mitochondrial size, carnitine-, FAO-, FA-signature, and protein levels of HMGCS and MFN2. The MCT-related findings support the previously reported beneficial effects of MCTs in rodents, such as the increase in LCFA β-oxidation and faster recovery from ischemia [26]. Indeed, the MCT induced elevated levels of activated FA species in the mouse plasma (e.g. acetylcarnitine and palmitolycarnitine), ready for mitochondrial import, support this data. In addition, we observed an LCT-dependent increase in C18:1 ω-9 FA towards SD, which was not present in the LCT/MCT group. This is especially interesting as the latter FA correlates with CVD risk and all-cause mortality in humans [74].

Previous data in rats showed that LCT-KDs of a lower 4:1 ketogenic ratio does not affect hearts after four weeks of feeding [40]. Others reported the development of cardiac fibrosis after 12 weeks of LCT-KD feeding (4:1 ketogenic ratio); however, they only analyzed obese mice with diabetic cardiomyopathy and not healthy controls [42]. Xu and colleagues reported that 16 weeks of an LCT-KD diet (4:1 ketogenic ratio) induced fibrosis in rats [41]. Thus, the feeding time frame might be a more important factor in the onset of cardiac changes than the ketogenic ratio per se. Mechanistically, You et al. [40] reported that LCT-KD induces the infiltration of immune cells in spontaneously hypertensive rats, which might contribute to inflammation and fibroblast activation. The authors showed that fibroblasts are co-activated with transforming growth factor-β and β-OHB *in vitro*. Tao et al. [42] observed reduced regulatory T cell plasma levels and cardiac fibrosis in the hearts of obese mice with diabetic cardiomyopathy after 12 weeks on a LCT-KD. The induction of fibroblasts by blunting the Interleukin-33/ST2L axis was discussed. In contrast, pathological assessment in our study did not reveal differences in the infiltration of immune cells, such as macrophages and T cells (data not shown), or an elevated oxidative stress response of proteins upon KD feeding. NRF2, stabilized by ROS, was even slightly reduced upon KD feeding, in line with the proposed anti-oxidative effects of β-OHB [75].

At the molecular level, we excluded the SIRT7/histone deacetylase 2/mitochondrial biogenesis axis as a mode of action of β-OHB in the rat heart upon LCT-KD feeding, as reported previously [41]. By using mitochondrial (mt)DNA/nuclear DNA ratios as a primary readout for mitochondrial mass, it was reported that β-OHB reduces mitochondrial mass in cardiomyocytes thereby producing an energy crisis in cells. However, basal and ATP-linked oxygen consumption rates per isolated rat cardiomyocyte, which both depend on the mitochondrial number per cell as well as individual mitochondrial activity, were indistinguishable from SD-fed rat cells, despite a 50% reduced mtDNA/DNA ratio. We want to stress that i) mtDNA levels can heavily fluctuate and should not solely be taken to assume mitochondrial mass [76]; and ii) the suggested response to the chemical uncoupler, carbonyl cyanide-p-trifluoromethoxyphenylhydrazone does not indicate ATP content, resting respiration, or membrane potential [77] because it only depicts uncoupled respiration activity. Accordingly, we suggest the data regarding mitochondrial bioenergetic measurements [41] need to be re-interpreted. Of note, previous reports showed that β-OHB levels heavily fluctuated under a KD in mice over a day [78], which must be taken into consideration when comparing studies.

We observed the induction of molecular markers of mitochondrial FA import, such as *Cpt1*, SLC25A20, and UCP3 as a marker of FAO upon LCT and LCT/MCT feeding. UCP3 was shown to inversely correlate with UCP2 protein levels upon increased heart maturation [45], and to be critically involved in cardiac energy homeostasis and FAO [26,79–82]. In addition, we observed that transcription of the mitochondrial rate-limiting ketolytic enzyme, *Oxct1,* was downregulated and the fate-committing enzyme of cardiac ketogenesis, *Hmgcs2,* was upregulated upon KD feeding. On the protein level, LCT-KD strongly induced HMGCS, and supplementation with MCT dampened this increase. Wentz and colleagues showed that chronic exposure to LCT-KD resulted in a myocardial response that reduced β-OHB utilization and preserved high rates of FAO but resulted in metabolic inflexibility [55]. Interestingly, increased HMGCS protein did not result in *de novo* cardiac ketogenesis. We speculate that the observed lower HMGCS protein levels in the LCT/MCT group is a molecular sign of residing flexibility and full-on FAO, as depicted by high UCP3 levels [45], and supported by the normal mitochondrial size, MFN2 levels and high amounts of activated FA-species in plasma. This is in line with the previously reported benefits of MCTs on LCFA β-oxidation [26]. Furthermore, we assume that this loss of metabolic flexibility of the heart after long-term KD could be an underlying cause of fibrosis, which would explain why a shorter 4-week KD period did not induce fibrosis at all as shown recently [40].

Adding of MCT to diets reduced white adipose tissue depots, in alignment with [83], where partial LCT replacement with MCT in high-fat diets led to improved metabolic features commonly associated with obesity. Furthermore, MCTs boosted mitochondrial UCP3 protein levels and the general FAO signature was stronger than in LCT-fed mice. Of note, LCT/MCT exclusively elevated transcripts of the FA sensor, *Pparγ1*, which, interestingly, was discussed as an anti-fibrotic, cardioprotective protein [30], possibly due to a compensatory mechanism. We found an LCT/MCT-related trend toward increased UCP3 protein levels compared to LCT feeding, most likely as a result of stronger mitochondrial FAO induction as MCT-derived FAs can bypass the SLC25A20/CPT2 axis. This was shown in leukocytes of patients with a complete loss of SLC25A20 that were still able to oxidize octanoate [84]. Octanoyl carnitine was shown to be metabolized in mitochondria in a CPT2-independent fashion [85]. Although positive and anti-inflammatory effects of MCTs [22–25] on cardiac health were previously reported, in our study, both LCT and LCT/MCT diets showed similar collagen deposition, and LCT/MCT tended to induce LD size beyond LCT levels. This suggests an increased oxidative burden by, for example, lipid species, which might be a link to the observed deleterious effects of MCTs in our psoriasis study. In this latter study, we observed increased infiltration of neutrophils and subsequently a worsened psoriatic response towards imiquimod [39].

Although the results from rodent studies are a cause for concern, the KD feeding regimen applied to treat epilepsy in children was reviewed as safe in terms of cardiac parameters [6,7]. In addition, the effects of a 6-week KD (2:1 ketogenic ratio) were generally favorable with regard to CVDs in men [19]. This implies that rodent KD ratios are possibly too high. However, human-like β-OHB levels are not reached under 8:1 ketogenic ratios.

Ketogenic diets were recently shown to increase health span and life span in mice [12,13]. However, the critical relationship between FA, KD, and health was revealed in a recent meta-study that showed increased mortality when carbohydrates were exchanged for animal-derived fat and protein in humans [86]. Therefore, one should cautiously evaluate the KD fat composition and duration.

 

Furthermore, our data strongly indicate that the mechanisms proposed in the literature (e.g. immune system stimulated fibroblast activation vs. cardiomyocyte apoptosis) depend strongly on the model and animal used. How animal studies can be sensitive to background is well known, and has been recently shown again by us in an aging study comparing C57/BL6N and C57/BL6J mice [87]. Future studies should focus on further variations in FA composition (e.g. reduction in ω-6 FA), time-frame and keto-cycling, as well as single cardiomyocyte analysis in fibrotic regions. They should also address structural—functional relationships as well as the *in vivo* bioenergetic status of cardiac tissue.

## AUTHORS' CONTRIBUTIONS

**Conceptualization:** F. S., E. E. P.; **Methodology:** F. S., T. B., K. D., B. K., E. E. P.; **Validation:** F. S., C. S., E. E. P.; **Formal analysis:** F. S., C. S.; **Investigation:** F. S., C. S., K. D., A. G., A. S, A. D.; **Resources:** F. S., K. D., I. W., B. K., V. S.; E. E. P.; **Writing — Original Draft:** F. S. **Writing — Review & Editing:** F. S., C.·S., K. D., B. K., E. E. P.; **Visualization:** F. S. **Supervision:** F. S., E. E. P.; **Project administration:** F. S. **Funding acquisition:** F. S. All authors have approved the final version of the manuscript.

## FUNDING

This study was supported by the University of Veterinary Medicine Vienna Start-up grant number PP15018136 (to F.S.).

## ETHICS APPROVAL STATEMENT

All animal experiments were approved by the Austrian national authority according to §§ 26ff. of the Animal Experiments Act.

## DATA AVAILABILITY

Data will be made available on request.

## ACKNOWLEDGMENTS

We thank Sarah Bardakji, Soleman Sasgary, Waltraud Tschulenk and Nikole Ginner for their excellent technical expertise, Maria Andreeva, Valeriya Panteva, Petra Kodajova and Katharina Granig for technical help, Sandra Högler for the support in pathological assessment, and Stefanie Hackl for processing of mouse plasma for metabolomics. This research was supported using resources of the VetCore Facility (Genomics) of the University of Veterinary Medicine Vienna.

## CONFLICT OF INTEREST

The authors declare no conflict of interest.

## APPENDIX A. SUPPLEMENTARY DATA

Supplementary data to this article can be found online at https://doi.org/10.1016/j.molmet.2023.101711.

## REFERENCES

[1] Travers JG, Kamal FA, Robbins J, Yutzey KE, Blaxall BC. Cardiac fibrosis: the fibroblast awakens. 2016.

[2] Taegtmeyer H, Young ME, Lopaschuk GD, Abel ED, Brunengraber H, Darley-Usmar V, et al. Assessing cardiac metabolism: a scientific statement from the American heart association. Circ Res 2016;118(10):1659—701.

[3] Wende AR, Brahma MK, McGinnis GR, Young ME. Metabolic origins of heart failure. JACC Basic Transl Sci 2017;2(3):297—310.

[4] Pellieux C, Montessuit C, Papageorgiou I, Pedrazzini T, Lerch R. Differential effects of high-fat diet on myocardial lipid metabolism in failing and nonfailing hearts with angiotensin II-mediated cardiac remodeling in mice. Am J Physiol Heart Circ Physiol 2012;302(9):H1795—805.

[5] Murashige D, Jang C, Neinast M, Edwards JJ, Cowan A, Hyman MC, et al. Comprehensive quantification of fuel use by the failing and nonfailing human heart. Science 2020;370(6514):364—8.

[6] Doksoz O, Guzel O, Yilmaz U, Isguder R, Celegen K, Mese T. Dispersion durations of P-wave and QT interval in children treated with a ketogenic diet. Pediatr Neurol 2014;50(4):343—6.

[7] Ozdemir R, Kucuk M, Guzel O, Karadeniz C, Yilmaz U, Mese T. Does ketogenic diet have any negative effect on cardiac systolic and diastolic functions in children with intractable epilepsy?: one-year follow-up results. Brain Dev 2016;38(9):842—7.

[8] Aminzadeh-Gohari S, Feichtinger RG, Vidali S, Locker F, Rutherford T, O'Donnel M, et al. A ketogenic diet supplemented with medium-chain triglycerides enhances the anti-tumor and anti-angiogenic efficacy of chemotherapy on neuroblastoma xenografts in a CD1-nu mouse model. Oncotarget 2017;8(39):64728—44.

[9] Weber DD, Aminzadeh-Gohari S, Tulipan J, Catalano L, Feichtinger RG, Kofler B. Ketogenic diet in the treatment of cancer - where do we stand? Mol Metabol 2020;33:102—21.

[10] Vidali S, Aminzadeh S, Lambert B, Rutherford T, Sperl W, Kofler B, et al. Mitochondria: the ketogenic diet-A metabolism-based therapy. Int J Biochem Cell Biol 2015;63:55—9.

[11] Hopkins BD, Pauli C, Du X, Wang DG, Li X, Wu D, et al. Suppression of insulin feedback enhances the efficacy of PI3K inhibitors. Nature 2018;560(7719):499—503.

[12] Roberts MN, Wallace MA, Tomilov AA, Zhou Z, Marcotte GR, Tran D, et al. A ketogenic diet extends longevity and healthspan in adult mice. Cell Metabol 2018;27(5):1156.

[13] Newman JC, Covarrubias AJ, Zhao M, Yu X, Gut P, Ng CP, et al. Ketogenic diet reduces midlife mortality and improves memory in aging mice. Cell Metabol 2017;26(3):547—557 e548.

[14] Yurista SR, Chong CR, Badimon JJ, Kelly DP, de Boer RA, Westenbrink BD. Therapeutic potential of ketone bodies for patients with cardiovascular disease: JACC state-of-the-art Review. J Am Coll Cardiol 2021;77(13):1660—9.

[15] Zhu H, Bi D, Zhang Y, Kong C, Du J, Wu X, et al. Ketogenic diet for human diseases: the underlying mechanisms and potential for clinical implementations. Signal Transduct Targeted Ther 2022;7(1):11.

[16] Kolb H, Kempf K, Rohling M, Lenzen-Schulte M, Schloot NC, Martin S. Ketone bodies: from enemy to friend and guardian angel. BMC Med 2021;19(1):313.

[17] Chu Y, Zhang C, Xie M. Beta-Hydroxybutyrate, friend or foe for stressed hearts. Frontiers in Aging 2021;2.

[18] Guo Y, Zhang C, Shang FF, Luo M, You Y, Zhai Q, et al. Ketogenic diet ameliorates cardiac dysfunction via balancing mitochondrial dynamics and inhibiting apoptosis in type 2 diabetic mice. Aging Dis 2020;11(2):229—40.

[19] Sharman MJ, Kraemer WJ, Love DM, Avery NG, Gomez AL, Scheett TP, et al. A ketogenic diet favorably affects serum biomarkers for cardiovascular disease in normal-weight men. J Nutr 2002;132(7):1879—85.

[20] Dyńka D, Kowalcze K, Ambrozkiewicz F, Paziewska A. Effect of the ketogenic diet on the prophylaxis and treatment of diabetes mellitus: a Review of the meta-analyses and clinical trials. Nutrients 2023;15(3):500.

[21] Jornayvaz FR, Jurczak MJ, Lee HY, Birkenfeld AL, Frederick DW, Zhang D, et al. A high-fat, ketogenic diet causes hepatic insulin resistance in mice,

 

despite increasing energy expenditure and preventing weight gain. Am J Physiol Endocrinol Metab 2010;299(5):E808–15.
[22] Geng S, Zhu W, Xie C, Li X, Wu J, Liang Z, et al. Medium-chain triglyceride ameliorates insulin resistance and inflammation in high fat diet-induced obese mice. Eur J Nutr 2016;55(3):931–40.
[23] Balietti M, Fattoretti P, Giorgetti B, Casoli T, Di Stefano G, Solazzi M, et al. A ketogenic diet increases succinic dehydrogenase activity in aging cardiomyocytes. Ann N Y Acad Sci 2009;1171:377–84.
[24] Papada E, Kaliora AC, Gioxari A, Papalois A, Forbes A. Anti-inflammatory effect of elemental diets with different fat composition in experimental colitis. Br J Nutr 2014;111(7):1213–20.
[25] Kono H, Fujii H, Asakawa M, Maki A, Amemiya H, Hirai Y, et al. Medium-chain triglycerides enhance secretory IgA expression in rat intestine after administration of endotoxin. Am J Physiol Gastrointest Liver Physiol 2004;286(6): G1081–9.
[26] Edwards KS, Ashraf S, Lomax TM, Wiseman JM, Hall ME, Gava FN, et al. Uncoupling protein 3 deficiency impairs myocardial fatty acid oxidation and contractile recovery following ischemia/reperfusion. Basic Res Cardiol 2018;113(6):47.
[27] Lima TI, Guimaraes D, Sponton CH, Bajgelman MC, Palameta S, Toscaro JM, et al. Essential role of the PGC-1alpha/PPARbeta axis in Ucp3 gene induction. J Physiol 2019;597(16):4277–91.
[28] Lee K, Kerner J, Hoppel CL. Mitochondrial carnitine palmitoyltransferase 1a (CPT1a) is part of an outer membrane fatty acid transfer complex. J Biol Chem 2011;286(29):25655–62.
[29] Pohl EE, Rupprecht A, Macher G, Hilse KE. Important trends in UCP3 investigation. Front Physiol 2019;10:470.
[30] Chandra M, Miriyala S, Panchatcharam M. PPARgamma and its role in cardiovascular diseases. PPAR Res 2017;2017:6404638.
[31] Makrecka-Kuka M, Sevostjanovs E, Vilks K, Volska K, Antone U, Kuka J, et al. Plasma acylcarnitine concentrations reflect the acylcarnitine profile in cardiac tissues. Sci Rep 2017;7(1):17528.
[32] Goldberg IJ, Reue K, Abumrad NA, Bickel PE, Cohen S, Fisher EA, et al. Deciphering the role of lipid droplets in cardiovascular disease: a report from the 2017 national heart, lung, and blood institute workshop. Circulation 2018;138(3):305–15.
[33] Catala A. Lipid peroxidation of membrane phospholipids generates hydroxy-alkenals and oxidized phospholipids active in physiological and/or pathological conditions. Chem Phys Lipids 2009;157(1):1–11.
[34] Malingriaux EA, Rupprecht A, Gille L, Jovanovic O, Jezek P, Jaburek M, et al. Fatty acids are key in 4-hydroxy-2-nonenal-mediated activation of uncoupling proteins 1 and 2. PLoS One 2013;8(10):e77786.
[35] Jovanovic O, Pashkovskaya AA, Annibal A, Vazdar M, Burchardt N, Sansone A, et al. The molecular mechanism behind reactive aldehyde action on transmembrane translocations of proton and potassium ions. Free Radic Biol Med 2015;89:1067–76.
[36] Mali VR, Palaniyandi SS. Regulation and therapeutic strategies of 4-hydroxy-2-nonenal metabolism in heart disease. Free Radic Res 2014;48(3):251–63.
[37] Sztalryd C, Brasaemle DL. The perilipin family of lipid droplet proteins: gatekeepers of intracellular lipolysis. Biochim Biophys Acta Mol Cell Biol Lipids 2017;1862(10 Pt B):1221–32.
[38] Wang H, Sreenivasan U, Gong DW, O'Connell KA, Dabkowski ER, Hecker PA, et al. Cardiomyocyte-specific perilipin 5 overexpression leads to myocardial steatosis and modest cardiac dysfunction. J Lipid Res 2013;54(4):953–65.
[39] Locker F, Leitner J, Aminzadeh-Gohari S, Weber DD, Sanio P, Koller A, et al. The influence of ketogenic diets on psoriasiform-like skin inflammation. J Invest Dermatol 2020;140(3):707–710 e707.
[40] You Y, Guo Y, Jia P, Zhuang B, Cheng Y, Deng H, et al. Ketogenic diet aggravates cardiac remodeling in adult spontaneously hypertensive rats. Nutr Metab 2020;17:91.
[41] Xu S, Tao H, Cao W, Cao L, Lin Y, Zhao SM, et al. Ketogenic diets inhibit mitochondrial biogenesis and induce cardiac fibrosis. Signal Transduct Targeted Ther 2021;6(1):54.
[42] Tao J, Chen H, Wang YJ, Qiu JX, Meng QQ, Zou RJ, et al. Ketogenic diet suppressed T-regulatory cells and promoted cardiac fibrosis via reducing mitochondria-associated membranes and inhibiting mitochondrial function. Oxid Med Cell Longev 2021;2021:5512322.
[43] Gregor A, Huber L, Auernigg-Haselmaier S, Sternberg F, Billerhart M, Dunkel A, et al. A comparison of the impact of restrictive diets on the gastrointestinal tract of mice. Nutrients 2022;14(15).
[44] Locker F, Vidali S, Holub BS, Stockinger J, Brunner SM, Ebner S, et al. Lack of galanin receptor 3 alleviates psoriasis by altering vascularization, immune cell infiltration, and cytokine expression. J Invest Dermatol 2018;138(1): 199–207.
[45] Hilse KE, Rupprecht A, Egerbacher M, Bardakji S, Zimmermann L, Wulczyn A, et al. The expression of uncoupling protein 3 coincides with the fatty acid oxidation type of metabolism in adult murine heart. Front Physiol 2018;9:747.
[46] Hilse KE, Kalinovich AV, Rupprecht A, Smorodchenko A, Zeitz U, Staniek K, et al. The expression of UCP3 directly correlates to UCP1 abundance in brown adipose tissue. Biochim Biophys Acta 2016;1857(1):72–8.
[47] Rich L. Collagen and Picrosirius red staining: a polarized light assessment of fibrillar hue and spatial distribution. Journal of Morphological Sciences 2005;22(2):97–104.
[48] Baumann T, Dunkel A, Schmid C, Schmitt S, Hiltensperger M, Lohr K, et al. Regulatory myeloid cells paralyze T cells through cell-cell transfer of the metabolite methylglyoxal. Nat Immunol 2020;21(5):555–66.
[49] Hofstetter CK, Dunkel A, Hofmann T. Unified flavor quantitation: toward high-throughput analysis of key food odorants and tastants by means of ultra-high-performance liquid chromatography tandem mass spectrometry. J Agric Food Chem 2019;67(31):8599–608.
[50] Just S, Mondot S, Ecker J, Wegner K, Rath E, Gau L, et al. The gut microbiota drives the impact of bile acids and fat source in diet on mouse metabolism. Microbiome 2018;6(1):134.
[51] Chambers MC, Maclean B, Burke R, Amodei D, Ruderman DL, Neumann S, et al. A cross-platform toolkit for mass spectrometry and proteomics. Nat Biotechnol 2012;30(10):918–20.
[52] Tautenhahn R, Bottcher C, Neumann S. Highly sensitive feature detection for high resolution LC/MS. BMC Bioinf 2008;9:504.
[53] Ritchie ME, Phipson B, Wu D, Hu Y, Law CW, Shi W, et al. Limma powers differential expression analyses for RNA-sequencing and microarray studies. Nucleic Acids Res 2015;43(7):e47.
[54] Vidali S, Aminzadeh-Gohari S, Feichtinger RG, Vatrinet R, Koller A, Locker F, et al. The ketogenic diet is not feasible as a therapy in a CD-1 nu/nu mouse model of renal cell carcinoma with features of Stauffer's syndrome. Oncotarget 2017;8(34):57201–15.
[55] Wentz AE, d'Avignon DA, Weber ML, Cotter DG, Doherty JM, Kerns R, et al. Adaptation of myocardial substrate metabolism to a ketogenic nutrient environment. J Biol Chem 2010;285(32):24447–56.
[56] Chen Y, Dorn 2nd GW. PINK1-phosphorylated mitofusin 2 is a Parkin receptor for culling damaged mitochondria. Science 2013;340(6131):471–5.
[57] LeBleu VS, O'Connell JT, Gonzalez Herrera KN, Wikman H, Pantel K, Haigis MC, et al. PGC-1alpha mediates mitochondrial biogenesis and oxidative phosphorylation in cancer cells to promote metastasis. Nat Cell Biol 2014;16(10):992–1003. 1001-1015.

 

[58] Garnier A, Fortin D, Delomenie C, Momken I, Veksler V, Ventura-Clapier R. Depressed mitochondrial transcription factors and oxidative capacity in rat failing cardiac and skeletal muscles. J Physiol 2003;551(Pt 2):491–501.
[59] Chen L, Gong Q, Stice JP, Knowlton AA. Mitochondrial OPA1, apoptosis, and heart failure. Cardiovasc Res 2009;84(1):91–9.
[60] Piquereau J, Caffin F, Novotova M, Prola A, Garnier A, Mateo P, et al. Down-regulation of OPA1 alters mouse mitochondrial morphology, PTP function, and cardiac adaptation to pressure overload. Cardiovasc Res 2012;94(3):408–17.
[61] Santin Y, Fazal L, Sainte-Marie Y, Sicard P, Maggiorani D, Tortosa F, et al. Mitochondrial 4-HNE derived from MAO-A promotes mitoCa(2+) overload in chronic postischemic cardiac remodeling. Cell Death Differ 2020;27(6):1907–23.
[62] Tonelli C, Chio IIC, Tuveson DA. Transcriptional regulation by Nrf2. Antioxidants Redox Signal 2018;29(17):1727–45.
[63] Dodson M, Castro-Portuguez R, Zhang DD. NRF2 plays a critical role in mitigating lipid peroxidation and ferroptosis. Redox Biol 2019;23:101107.
[64] Ahmed SM, Luo L, Namani A, Wang XJ, Tang X. Nrf2 signaling pathway: pivotal roles in inflammation. Biochim Biophys Acta, Mol Basis Dis 2017;1863(2):585–97.
[65] Milder JB, Liang LP, Patel M. Acute oxidative stress and systemic Nrf2 activation by the ketogenic diet. Neurobiol Dis 2010;40(1):238–44.
[66] Mullebner A, Moldzio R, Redl H, Kozlov AV, Duvigneau JC. Heme degradation by heme oxygenase protects mitochondria but induces ER stress via formed bilirubin. Biomolecules 2015;5(2):679–701.
[67] Postl A, Zifko C, Hartl RT, Ebel T, Miller I, Moldzio R, et al. Transient increase of free iron in rat livers following hemorrhagic-traumatic shock and reperfusion is independent of heme oxygenase 1 upregulation. Shock 2011;36(5):501–9.
[68] Gozzelino R, Jeney V, Soares MP. Mechanisms of cell protection by heme oxygenase-1. Annu Rev Pharmacol Toxicol 2010;50:323–54.
[69] Loboda A, Damulewicz M, Pyza E, Jozkowicz A, Dulak J. Role of Nrf2/HO-1 system in development, oxidative stress response and diseases: an evolutionarily conserved mechanism. Cell Mol Life Sci 2016;73(17):3221–47.
[70] Shan H, Li T, Zhang L, Yang R, Li Y, Zhang M, et al. Heme oxygenase-1 prevents heart against myocardial infarction by attenuating ischemic injury-induced cardiomyocytes senescence. EBioMedicine 2019;39:59–68.
[71] Scher MB, Vaquero A, Reinberg D. SirT3 is a nuclear NAD+-dependent histone deacetylase that translocates to the mitochondria upon cellular stress. Genes Dev 2007;21(8):920–8.
[72] Ansari A, Rahman MS, Saha SK, Saikot FK, Deep A, Kim KH. Function of the SIRT3 mitochondrial deacetylase in cellular physiology, cancer, and neurodegenerative disease. Aging Cell 2017;16(1):4–16.
[73] Traba J, Kwarteng-Siaw M, Okoll TC, Li J, Huffstutler RD, Bray A, et al. Fasting and refeeding differentially regulate NLRP3 inflammasome activation in human subjects. J Clin Invest 2015;125(12):4592–600.
[74] Steffen BT, Duprez D, Szklo M, Guan W, Tsai MY. Circulating oleic acid levels are related to greater risks of cardiovascular events and all-cause mortality: the Multi-Ethnic Study of Atherosclerosis. J Clin Lipidol 2018;12(6):1404–12.
[75] Youm YH, Nguyen KY, Grant RW, Goldberg EL, Bodogai M, Kim D, et al. The ketone metabolite beta-hydroxybutyrate blocks NLRP3 inflammasome-mediated inflammatory disease. Nat Med 2015;21(3):263–9.
[76] Filograna R, Mennuni M, Alsina D, Larsson NG. Mitochondrial DNA copy number in human disease: the more the better? FEBS Lett 2021;595(8):976–1002.
[77] Zhdanov AV, Waters AH, Golubeva AV, Dmitriev RI, Papkovsky DB. Availability of the key metabolic substrates dictates the respiratory response of cancer cells to the mitochondrial uncoupling. Biochim Biophys Acta 2014;1837(1):51–62.
[78] Tognini P, Murakami M, Liu Y, Eckel-Mahan KL, Newman JC, Verdin E, et al. Distinct circadian signatures in liver and gut clocks revealed by ketogenic diet. Cell Metabol 2017;26(3):523–538 e525.
[79] Harmancey R, Vasquez HG, Guthrie PH, Taegtmeyer H. Decreased long-chain fatty acid oxidation impairs postischemic recovery of the insulin-resistant rat heart. Faseb J 2013;27(10):3966–78.
[80] Ozcan C, Palmeri M, Horvath TL, Russell KS, Russell 3rd RR. Role of uncoupling protein 3 in ischemia-reperfusion injury, arrhythmias, and preconditioning. Am J Physiol Heart Circ Physiol 2013;304(9):H1192–200.
[81] Perrino C, Schiattarella GG, Sannino A, Pironti G, Petretta MP, Cannavo A, et al. Genetic deletion of uncoupling protein 3 exaggerates apoptotic cell death in the ischemic heart leading to heart failure. J Am Heart Assoc 2013;2(3):e000086.
[82] Nabben M, van Bree BWJ, Lenaers E, Hoeks J, Hesselink MKC, Schaart G, et al. Lack of UCP3 does not affect skeletal muscle mitochondrial function under lipid-challenged conditions, but leads to sudden cardiac death. Basic Res Cardiol 2014;109(6):447.
[83] Rial SA, Jutras-Carignan A, Bergeron KF, Mounier C. A high-fat diet enriched in medium chain triglycerides triggers hepatic thermogenesis and improves metabolic health in lean and obese mice. Biochim Biophys Acta Mol Cell Biol Lipids 2020;1865(3):158582.
[84] Niezen-Koning KE, van Spronsen FJ, Ijlst L, Wanders RJ, Brivet M, Duran M, et al. A patient with lethal cardiomyopathy and a carnitine-acylcarnitine translocase deficiency. J Inherit Metab Dis 1995;18(2):230–2.
[85] Pereyra AS, Harris KL, Soepriatna AH, Waterbury QA, Bharathi SS, Zhang Y, et al. Octanoate is differentially metabolized in liver and muscle and fails to rescue cardiomyopathy in CPT2 deficiency. J Lipid Res 2021;62:100069.
[86] Seidelmann SB, Claggett B, Cheng S, Henglin M, Shah A, Steffen LM, et al. Dietary carbohydrate intake and mortality: a prospective cohort study and meta-analysis. Lancet Public Health 2018;3(9):e419–28.
[87] Locker F, Bieler L, Nowack LMF, Leitner J, Brunner SM, Zaunmair P, et al. Involvement of neuropeptide galanin receptors 2 and 3 in learning, memory and anxiety in aging mice. Molecules 2021;26(7).

 